

Wall material effects in stationary plasma thrusters.

I. Parametric studies of an SPT-100

N. Gascon^{a)} and M. Dudeck

Laboratoire d'Aérothermique, Centre National de la Recherche Scientifique, 45071 Orléans, France

S. Barral

Institute of Fundamental Technological Research, Polish Academy of Science, 00049 Warsaw, Poland

(Received 3 September 2002; accepted 15 July 2003)

The operation of a laboratory version of the flight-qualified SPT-100 stationary plasma thruster is compared for four different discharge chamber wall materials: a boron nitride–silica mixture (borosil), alumina, silicon carbide, and graphite. The discharge is found to be significantly affected by the nature of the walls: changes in operating regimes, up to 25% variations of the mean discharge current, and over 100% variations of the discharge current fluctuation amplitude are observed between materials. Thrust, however, is only moderately affected. Borosil is the only material tested that allows operating the thruster at a low mean current, low fluctuation level and high thrust efficiency regime. It is suggested that secondary electron emission under electron bombardment is the main cause of the observed differences in discharge operation, except for graphite, where the short-circuit current inside the walls is believed to play a major role. It is also suggested that the photoelectric effect, which has apparently not been given attention before in the Hall thruster literature, could increase the cross-field electron current. © 2003 American Institute of Physics. [DOI: 10.1063/1.1611880]

I. INTRODUCTION

A. Historical perspective

Hall thrusters are cross-field plasma sources that can be used as rocket engines with performance well suited for station-keeping and orbit transfer of satellites. The Hall thruster appeared independently in the USA and in the former Soviet Union in the late 1950s, deriving from ongoing works on magnetrons.^{1,2} The principle of Hall thruster operation is to impose on a plasma discharge a magnetic field of appropriate intensity, such that the resulting electron Hall parameter $\omega_c \tau_e$ be much greater than unity, and the ion cyclotron radius much larger than the characteristic dimension of the discharge. Under such conditions, the self-consistent electric field created by the retarded electron flow accelerates in turn the ions, which are not magnetized due to their higher inertia.

It was early recognized that the type of material used for the walls of the discharge chamber (also called channel) had a significant impact on the characteristics of the plasma and on the ion acceleration process. In most of the first published works on Hall thrusters the channel had electrically insulating walls (e.g., made of quartz³ or coated with alumina⁴), with lengths comparable to the channel width. In such a discharge, due to the high electric conductivity perpendicularly to the channel walls (i.e., along the magnetic field lines), the high energy electrons are continuously replaced by low energy secondary electrons, resulting in a limitation of electron

temperature and temperature gradients to moderate values. Ion acceleration takes place in a quasineutral plasma over distances much larger than the electron cyclotron radius or the Debye length. This type of Hall thruster is also called thruster with magnetic layer⁵ (TML), thruster with extended acceleration zone,⁶ and most commonly now stationary plasma thruster (SPT). In another variant of the Hall thruster,⁷ the channel walls are electrically conducting, biased to the cathode potential and much shorter than the channel width. In this configuration, the electrons retain most of their energy as they flow towards the anode, allowing steep electron temperature gradients and high electron temperatures. The ions are accelerated in a space-charge limited sheath located close to the anode, with a characteristic acceleration length of about the same size as the electron cyclotron radius. The initial denomination of space-charge sheath thruster⁷ was rapidly abandoned in favor of thruster with anode layer⁵ (TAL).

During the 1970s, the Hall thruster was largely neglected in the USA, where electric propulsion research was essentially focused on the gridded ion thruster, which offered better performance for the interplanetary missions considered at the time.² In the Soviet Union, on the other hand, the research and development efforts on Hall thrusters continued intensively and led to the use of these device on numerous Soviet spacecraft, starting in 1972.^{8–10} An impressive body of research and technology was accumulated over two decades, but some of the related literature was published only in Russian and remained little known to western scientists.

The revival of U.S. interest in Hall thrusters was initiated in the 1980s by Kaufman^{11,12} (who, interestingly, is also one of the most prominent figures of gridded ion thruster

^{a)}Present address: Mechanical Engineering Department, Stanford University, Stanford, California 94305-3032; electronic mail: nicolas@navier.stanford.edu

research), and in the early 1990s, groups of U.S. scientists started a technology transfer program that included extensive ground tests at NASA centers with the commercial SPT-100 thruster, made by the Russian design bureau Fakel.^{13–15} The SPT-100 had channel walls made of borosil, a ceramic composed of a mixture of boron nitride and silica. Since this thruster was designed to serve onboard spacecraft, it can be assumed that the use of borosil resulted at the time in the most appropriate performance, in terms of thrust efficiency and lifetime (the channel had to resist the wear due to thermal and mechanical stress and to high energy ion bombardment⁵).

Even as Hall thruster research took momentum in the 1990s, the experimental literature covering the effects of walls on Hall thruster operation and performance remained scarce. One of the most remarkable works in this area was led by Bugrova¹⁶ with the aim of verifying some predictions of the so-called near-wall conductivity theory developed by Morozov.¹⁷ Among other findings, a clear correlation was established between the degree of roughness of the channel walls and the discharge current value. More recent studies were rather concerned with the nature of the wall material. In Ref. 18, sets of clean boron nitride (BN) walls were progressively coated with either quartz or stainless steel during thruster operation. With both types of coatings, it was observed that the acceleration region became narrower and the ion current density in the plume decreased. In Ref. 19, the whole BN coaxial cylinders originally constituting the discharge chamber were replaced with ones made of a machinable glass ceramic. As a result, for some values of the operating parameters, and in particular at high applied voltages or high magnetic flux intensities, the electron current was found to be significantly increased (as much as 30%), although the ion current in the plume and the thrust remained mostly unaffected. In Ref. 20, BN was compared with diamond. The new material was found to cause a narrowing of the range of stable operation, and a decrease of about 20% in both the electron current and the ion current. Finally, in some other works that specifically aimed at improving stationary plasma thruster performance,^{21–23} it was shown that the use of floating or biased conducting inserts in the channel walls of stationary plasma thrusters allows modifying the ion acceleration process and reducing the ion plume divergence. References 18–23 suggested qualitative explanations of the results with arguments involving the secondary electron emission (SEE) by the walls under electron bombardment.

B. Motivation and scope

A high priority has been put by the Centre National d'Etudes Spatiales (French Space Agency) on developing Hall thruster technology.²⁴ To this end, a research group on plasma propulsion was created in 1996 with the aerospace company Snecma and the scientific institutions Centre National de la Recherche Scientifique and Office National d'Etudes et de Recherches Aérospatiales. A space simulation facility, PIVOINE, was built in Orléans, France,²⁵ and specific diagnostics were developed.^{26,29} Based on the experience Snecma had gained from a close collaboration with

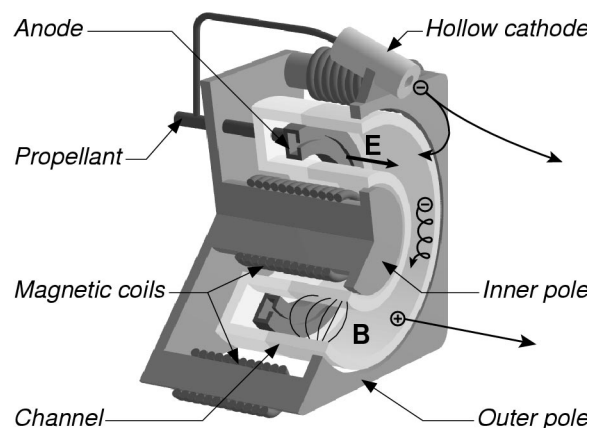


FIG. 1. Schematic cutaway view of the SPT-100ML. The channel outer diameter is 100 mm.

Fakel,²⁷ a laboratory SPT-100 thruster named SPT100-ML was fabricated. Over the years, a considerable amount of practical knowledge of the PIVOINE facility and of the SPT100-ML has been accumulated.^{25,26,28–30}

In this paper, we address the question of how a particular type of material can affect the operating regime and thrust efficiency of the stationary plasma thruster. After a presentation of the test facility in Sec. II, the different operating regimes of the SPT100-ML are characterized in Sec. III A. This classification expands and refines a previous one³⁰ in light of a new parametric investigation of the SPT100-ML with different channel wall materials. We also observe that although the type of wall material can significantly affect the discharge current, thrust remains relatively unchanged. In Sec. III B, we estimate the fraction of discharge current resulting from plasma–wall interactions, and suggest some effects related to wall materials that could be at the origin of the observed discharge operating regimes. Our goal here is not to propose a detailed theory of channel wall effects (this will be the subject of a companion paper³¹) but rather, to clarify some aspects of Hall thruster discharge behavior and to present an overview of the physical processes potentially involved.

II. TEST FACILITY

A. Thruster

A schematic view of the SPT-100ML thruster used in the experiments is given on Fig. 1.

In base configuration, The SPT100-ML is identical to the SPT-100 in terms of discharge chamber geometry, magnetic circuit and gas injector configuration, channel wall material, propellant, discharge operation and performance,^{13–15,25,28} but several features have been modified from the original design to facilitate parametric studies and the use of diagnostics. In particular, the coaxial channel cylinders can easily be changed. Four sets of channels walls are used in this study: the reference one is made of borosil (BN–SiO₂), and the other three are made of alumina (Al₂O₃), silicon carbide (SiC), and graphite (C). The motivation for using those materials derived in part from thruster lifetime considerations,

looking for low sputtering yields under ion bombardment, but this aspect of plasma-wall interactions is not addressed in the present work. Also, it should be noted that graphite is an electric conductor. With this wall material, knowing that the walls are left electrically floating during thruster operation, the SPT100-ML configuration is distinct from the TAL and TML cases described in the introduction. As mentioned in Ref. 5, however, previous studies conducted in the former Soviet Union showed that a stationary plasma thruster operates in a similar fashion with dielectric or floating conducting walls.^{32,33} In particular, the acceleration zone remains extended and electrically quasineutral, a clear difference from the TAL configuration.

The annular gas injector, located in the bottom plane of the channel, also serves as the anode. As with most modern ion thrusters, xenon is the propellant of choice, due to its low ionization potential, weak interaction with spacecraft environment, and a high density that minimizes storage constraints. Moreover, the large atomic mass of xenon allows avoiding the low thrust-to-power ratio associated with high specific impulses. The magnetic field is generated by five induction coils (four peripheral coils and one inner coil) and an iron core circuit. In the original SPT-100, the five magnetic coils are in series with the discharge. With the SPT100-ML, it is possible to use three independent power supplies for the discharge, the inner coil and the four outer coils (which remain in series). By varying the electric current in the magnetic coils, the magnetic flux intensity and the shape of the magnetic field lines can be modified, which could be interesting for a precise optimization of the performance.^{5,34} In the present study, however, the currents in all coils are set to the same values, so that the field lines do not change as the flux intensity varies. A hollow cathode provides electrons for establishing the discharge and for neutralizing the ion beam. The discharge electrodes and the magnetic circuit are electrically isolated when the discharge is off, and they are floating relatively to the vacuum chamber (ground) potential when the discharge is on.

The SPT-100ML operates nominally with a total xenon mass flow rate of 5.42 mg/s (5 mg/s for the main discharge and 0.42 mg/s for the hollow cathode), an applied voltage of 300 V, and 4.5 A of current in the magnetic circuit, which then generates a flux intensity of about 20 mT at the channel exit. Under such conditions, the SPT100-ML delivers a thrust of 80 mN with an efficiency close to 50% and an input power of 1.35 kW. Note that due to the saturation of the ferromagnetic circuit, the relation between the coil current and the magnetic flux intensity is linear only up to 5 A, although it remains monotonic above that value.

The thruster can withstand continuous thermal power up to 2 kW, which sets another limit on the range of investigation.

B. Vacuum chamber and diagnostics

The PIVOINE French test facility for plasma propulsion is described in details elsewhere.^{25,28} It was specially designed and scaled for SPT-100 studies, benefitting from the collaboration between Snecma and Fakel, and from the ex-

perience accumulated during U.S. test programs.¹³⁻¹⁵ The vacuum chamber of PIVOINE is a stainless steel nonmagnetic cylinder, 2.2 m in diameter, 4 m long, and 1 cm thick. The pumping down sequence is entirely automated: first, a rough vacuum is obtained with a four-stage rotative dry pump and a roots pump; once a pressure of $5 \cdot 10^{-3}$ mbar is attained, the cryogenic pump is started; it allows reaching a limit pressure of $5 \cdot 10^{-7}$ mbar. When the SPT100-ML runs at the nominal operating point (5.42 mg/s of xenon flow rate and 1.35 kW of discharge power), the pumping speed is 44 000 l/s and the pressure inside the vacuum chamber is $2.4 \cdot 10^{-5}$ mbar. Under such conditions, the interactions of the plasma jet with the vacuum chamber and the effects of backstreaming xenon particles on the discharge can be neglected, which results in a good simulation of the space environment.^{14,28} During thruster operation, cold cathode gauges and ionization gauges placed at several locations inside the vacuum chamber are used to measure pressure. The residual gas composition is continuously analyzed and monitored with a quadrupole mass spectrometer, and recorded regularly.

The two gas lines that feed the discharge and the hollow cathode are regulated by MKS flow controllers that have an upper limit of 65.5 sccm of Xe for the anode-injector, and 13.1 sccm of Xe for the cathode-neutralizer, with an accuracy of 1% of the full scale. The pressures downstream of the flow controllers are monitored with piezoelectric gauges.

The thruster discharge, the magnetic coils, and the hollow cathode heater each have their own power supply, with the following characteristics: (EMS 600-8-08-06) 0–600 V, 0–8 A range, 1 V steps as voltage generator for the discharge, and (ASF 400 20-20) 0–20 V, 0–20 A range, 0.2 A steps as current generator for the magnetic field coils and the cathode heater, respectively. They are all switching supplies, with a base switch frequency of 49.9 kHz. The discharge power supply is protected from the strong current peaks that can occur in the plasma by a RLC low-pass filter with a 3 kHz cutoff frequency. More details on the SPT100-ML power processing unit can be found in Ref. 30.

The axial thrust of the SPT100-ML is measured with a specially designed pendulum-type scale, described in Ref. 28. The integrated calibration system showed an excellent linearity and better than 0.5% reproducibility at rest (discharge off) in the 1–500 mN range, and it can be used during thruster operation. Numerous and repetitive uses of the thrust stand under various configurations and discharge operating conditions of the SPT100-ML and other Hall thrusters have demonstrated a 2% accuracy of thrust measurement.

The discharge current dc value and fluctuations are measured with a contactless current transducer (made in Switzerland by LEM, model LA25-NP), which has better than 0.5% accuracy and a bandwidth (-3 dB) of 0–150 kHz. The resulting time-varying voltage goes through a Tektronix VX4780 signal conditioner card that can provide at least 10 dB of active low-pass filtering for noise attenuation and antialiasing. The output is then digitized with a Tektronix VX4244 card that has 16 bits of maximum vertical resolution, and finally, the signal is recorded on a computer for further analysis. In the present study, the discharge current sampling

rate is 200 kS/s and all the records are 2048 samples (10.24 ms) long. Power spectrum estimators of the signals are obtained following Welch's classical method:³⁵ each record is divided into four nonoverlapping pieces, and a Hanning window is applied on every piece to minimize the Gibbs phenomenon; the Fourier spectra of the windowed time series are then averaged to estimate the signal power spectrum. The free parameters of the method are chosen as a compromise between, on the one hand, noise filtering and statistical robustness, and on the other hand, the ability to distinguish detailed features in the spectra.

During thruster operation, the following parameters are continuously measured, monitored on a computer and recorded with a data logger system: pressure inside the chamber and in the gas feed lines, gas flow rates (anode-injector and cathode-neutralizer), magnetic coil current and voltage, discharge voltage and current (dc values), thrust, cathode potential, cathode heater current, temperature inside the iron core of the inner electromagnet (which is the hottest region in the thruster structure).

III. RESULTS AND DISCUSSION

A. Performance and discharge operation

1. Overview

In all the results reported here, the working gas is xenon (research grade, 99.995% pure). When they are not specified, the SPT100-ML operating parameters are set to their nominal values, i.e., xenon flow rate at the anode $Q_{Xe} = 5$ mg/s, coil current $I_B = 4.5$ A, applied voltage $U_d = 300$ V. The cathode mass flow rate is kept constant at 0.42 mg/s throughout the study.

Such experiments in a simulated space environment require that the thruster be outgassed prior to the testing of a new set of channel walls.¹⁴ This is realized by putting the SPT100-ML 12 h in rough vacuum, then letting it stay 10 more hours inside the PIVOINE chamber while the cryogenic pump cools down and the pressure goes from $5 \cdot 10^{-3}$ mbar down to $5 \cdot 10^{-7}$ mbar. Every time the discharge is started after being off for more than one hour, it is run for at least one hour at the nominal operating point for thermal stabilization (and further outgassing, if need be). The operating parameters of the test facility and of the thruster (pressure, discharge current, etc.) are then checked against reference values.

For every channel wall material tested, the first day of experiments is devoted to an exploration of the discharge operating envelope. Then the thruster is left in vacuum overnight, and the second day several series of measurements are realized, varying one operating parameter (discharge voltage, coil current or xenon flow rate) at a time. Each measurement series is started at the nominal operating point. The test facility and thruster parameters are checked against reference values. Then the chosen operating parameter is varied, starting with values that result in the highest discharge power, i.e., high voltage, high flow rate or low coil current, respectively. Every time a new operating point is set, the discharge is considered stabilized at this point when the discharge current dc value and rms fluctuation power do not change more

than 5% for at least 5 min. The series is ended by a return to nominal operation and checks. The experiments dealing with the thrust and efficiency of the SPT100-ML are conducted separately from the discharge current characteristics series.

Figure 2 depicts typical discharge current characteristics of the SPT100-ML as functions of coil current (left column) or applied voltage (right column) for all tested materials. The maxima (resp. minima) correspond to records where 5% of the highest (resp. lowest) values were removed, to prevent the risk of abnormal extrema (caused by noise in the power supply, for example). For the same series of measurements, the discharge current fluctuation spectra are shown in Fig. 3. At every operating point, the spectrum is normalized to the total rms fluctuation power at this point. Therefore, only the frequency distributions can be compared between operating points, not the exact values of the power densities.

A series of measurements with the borosil walls, a coil current of $I_B = 4.5$ A and a xenon flow rate of $Q_{Xe} = 3.5$ mg/s was given a similar treatment, the results being shown in Figs. 4 and 5. The relevant discharge operating regime numbers (see Sec. III A 2, below) are also indicated in these two figures. The advantages of operating at this lower flow rate are a wider range of observable regimes and lower thermal stress on the thruster.

It should be noted that when the power supply voltage is set to a certain value (the *applied* voltage), the actual potential difference between the anode and the cathode (the *discharge* voltage) can be unsteady. Most of the discharge fluctuation power goes to the RLC filter, except in some operating regimes briefly discussed below.

The general features of the mean discharge current curves are typical for a modern stationary plasma thruster:^{5,36} first, the direct relation between the magnetic flux intensity and the electric resistance within the discharge is apparent in the left column of Fig. 2. Note that for all materials except alumina, the mean discharge current reaches a plateau at high coil currents. This is consistent with previous stationary plasma thruster studies, which also showed that when the magnetic field is further increased, the discharge reaches a point where it becomes highly unstable or can even self-extinct, then the discharge current saturates at a higher value due to anomalous conduction mechanisms.^{5,37}

The shape of the current–voltage ($I-V$) characteristics is also well-known: first, a rapid rise (ionization branch), followed by a narrow inflexion region, a plateau (or just a slight augmentation of the current), and finally an increase. In the ionization branch, the rapid augmentation in discharge current with increased voltage is due to the increase in mean electron energy, resulting in higher ionization rate and ionization fraction (avalanche ionization). In the plateau branch and for higher voltages, the ionization fraction has reached a maximum value and the ion current remains constant. Therefore, the increase in discharge current observed at high applied voltages can be attributed solely to changes in electron mobility. Note that the ionization fraction is always low in Hall thrusters (some 10% at most^{39,40}) but the propellant utilization, i.e., the conversion of injected neutral mass flow rate into an ionized jet at the exhaust, can reach over 90%.^{5,34} This is due to the considerable difference between the neutral

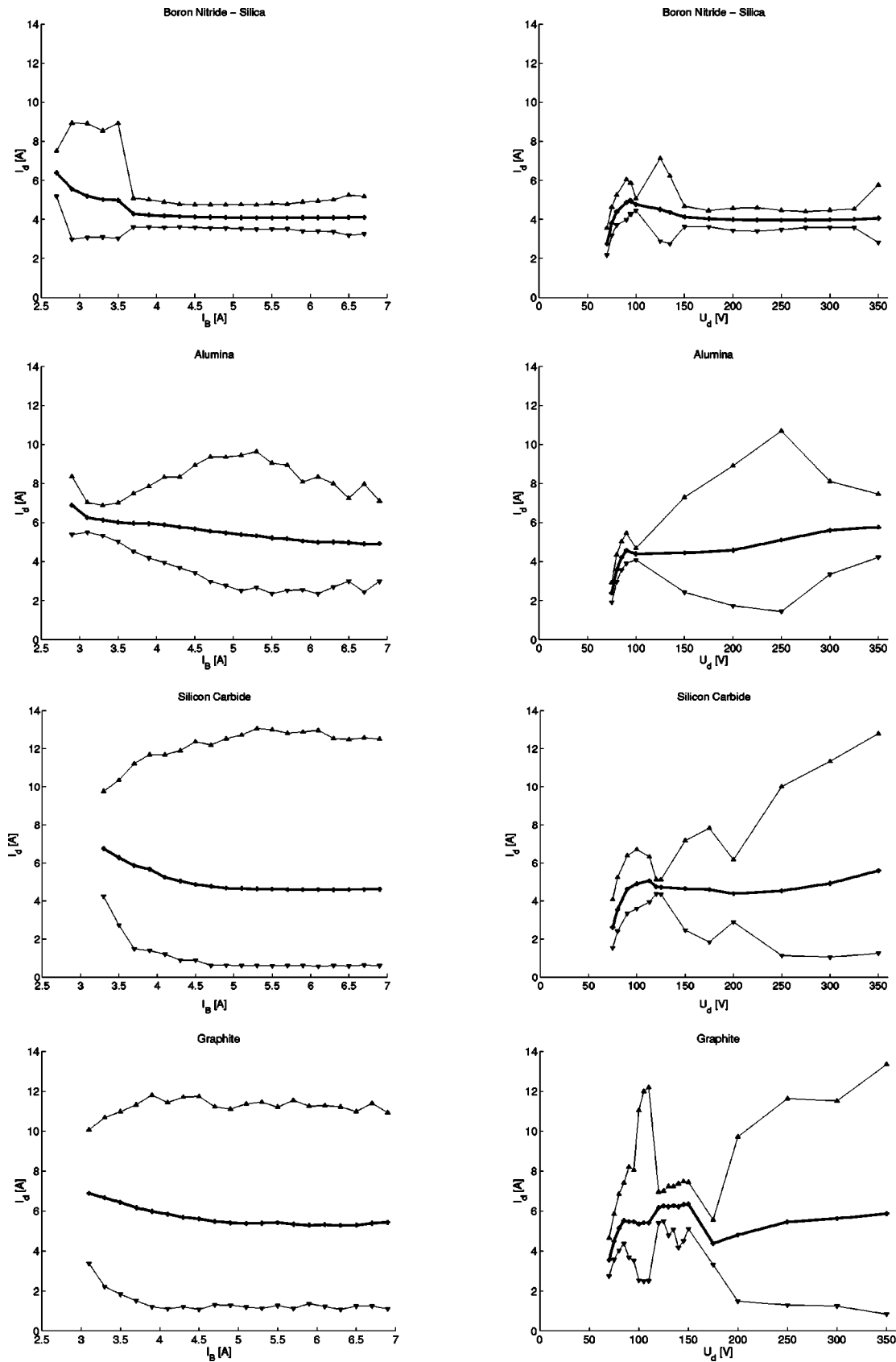


FIG. 2. Discharge current mean values (crosses) and fluctuation extrema (triangles). Xenon flow rate: 5 mg/s at the anode. In the left column, the applied voltage is set to 300 V, and the only variable parameter is the coil current. In the right column, the coil current is set to 4.5 A, and the only variable parameter is the applied voltage.

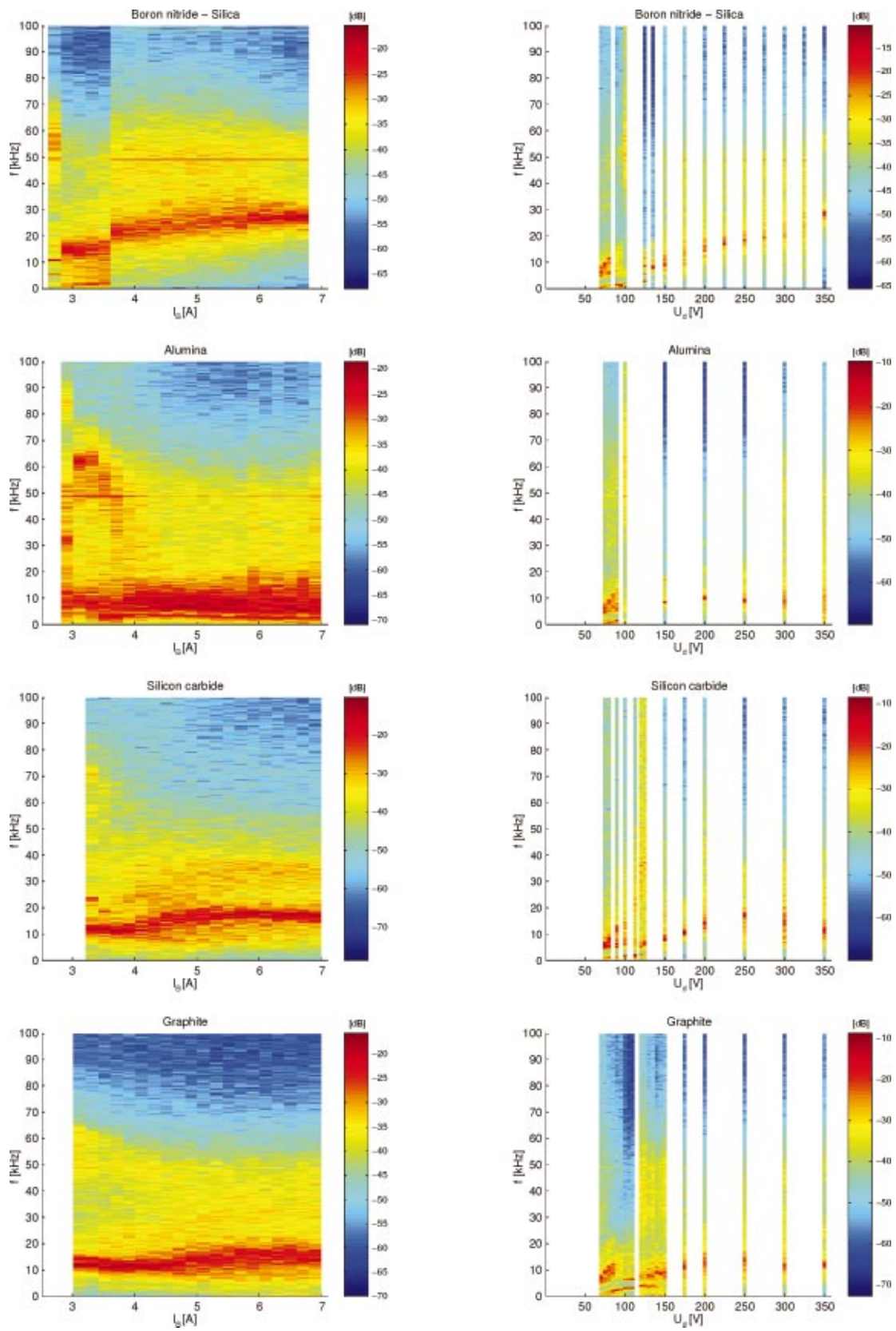


FIG. 3. (Color) Discharge current power spectra. The operating conditions correspond to Fig. 2. Every spectrum is normalized to the total fluctuation power at the corresponding operating point. The strong peak near 50 kHz present in several spectra (see also Fig. 5) is caused by the switching power supply.

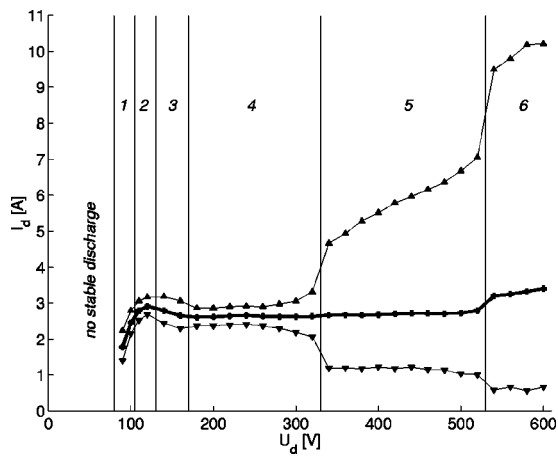


FIG. 4. Current–voltage characteristic (crosses) and extrema of the discharge current fluctuations (triangles) of the SPT100-ML. Borosil walls. Xenon flow rate at the anode: $Q_{Xe} = 3.5$ mg/s. Coil current: $I_B = 4.5$ A. The numbers on top refer to operating Regimes 1–6, described in the text.

velocity (200–400 m/s) and the ion velocity (10–20 km/s). At present, there is no satisfactory explanation given in the Hall thruster literature about the appearance of the negative resistance region in the $I-V$ characteristics, located near 100–150 V in the left panes of Fig. 2 and in Fig. 4, even though it seems to be a general feature of modern Hall thruster behavior.

As mentioned above, the $I-V$ characteristics were realized from high to low applied voltages. For the measurements presented in the right panels of Fig. 2 and Fig. 3 and in Fig. 4, the discharge was actually operated down to lower voltages than the lowest values shown on those plots, but it was then unstable and would self-extinct after a few minutes.

2. Operating regimes

It is beyond the scope of the present article to explain all the features that can be observed in Figs. 2–5. Nevertheless, as a guide for future studies, it can be useful to describe those features.

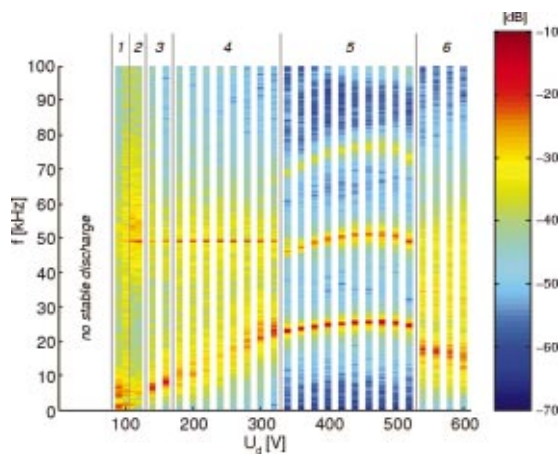


FIG. 5. (Color) Spectra of discharge current fluctuations as a function of the applied voltage. The operating conditions correspond to those of Fig. 4. Every spectrum is normalized to the total fluctuation power at the corresponding applied voltage. The numbers on top refer to operating Regimes 1–6.

The first major classification of operating regimes and plasma oscillations in stationary plasma thrusters was proposed in the 1970s by Tilinin,³⁷ and was the basis of a recent overview by Choueiri.³⁸ In these two articles, the control parameter was the radial magnetic induction at the center of the channel exit and the discussions were supported by measurements of the plasma density fluctuations over a wide range of frequencies (1 kHz–400 MHz), and by typical time-averaged values of the local plasma parameters. It should be noted, however, that these experimental data were collected on stationary plasma thrusters with older designs than the SPT-100 and more importantly, with only one type of channel wall material. It seems nonetheless possible to relate some of our results to Tilinin’s and Choueiri’s works.

As a first step, we can examine the left column of Figs. 2 and 3 and tentatively assign the relevant operating regimes:

- (a) Borosil walls. $I_B = 2.7$ A, regime IIIa (transition regime without electron drift wave). $I_B = 2.9-3.3$ A, regime IIIb (transition regime with weak electron drift wave). $I_B = 3.5-6.7$ A, regime IV (optimum regime);
- (b) Alumina walls. $I_B = 2.9$ A regime II (regular electron drift wave regime), $I_B = 3.1-3.7$ A, regime IIIa. $I_B = 3.9-6.9$ A, regime IIIb;
- (c) Silicon carbide walls. $I_B = 3.3-3.5$ A, regime IIIa. $I_B = 3.7-6.9$ A, regime IIIb;
- (d) Graphite walls. $I_B = 3.1-3.3$ A, regime IIIa. $I_B = 3.5-6.9$ A, regime IIIb.

With the exception of borosil, relating the discharge operation features to Tilinin’s classification is difficult, and the operating regimes tend to overlap. It can be noted, however, that borosil is the only wall material that offers the possibility of an “optimum” regime IV.

Next, following a previous study of the SPT100-ML,³⁰ we propose to characterize the discharge operating regimes by their position on the $I-V$ characteristic and the amplitude and spectrum of discharge current fluctuations.

In Figs. 2–5, up to six different operating regimes can be identified (we do not consider the self-extinction regime at low applied voltages). Other series of measurements conducted at low xenon flow rate revealed a seventh regime appearing at high voltages. Typical discharge current oscillograms of Regimes 1–7 are shown in Fig. 6.

Referring to Figs. 2–6, and moving our attention from low to high applied voltages, we note the following features:

Regime 1: In the ionization branch of the $I-V$ characteristics, the discharge fluctuations amplitude is moderate to high compared to the dc current (10%–50%). Apart from a frequency peak at 3 kHz resulting from interactions with the RLC filter, the strongest fluctuation activity, between 5–15 kHz, can be attributed at such low voltages to the so-called “spoke” instability^{3,41} that is believed to contribute to electron transport to the anode. As in Ref. 41, the frequency range of this instability shifts to higher values as the applied voltage is increased.

Regime 2: This regime appears around the inflexion point of the $I-V$ characteristics. It seems that the spoke instability is present, albeit weaker than in Regime 1, and the

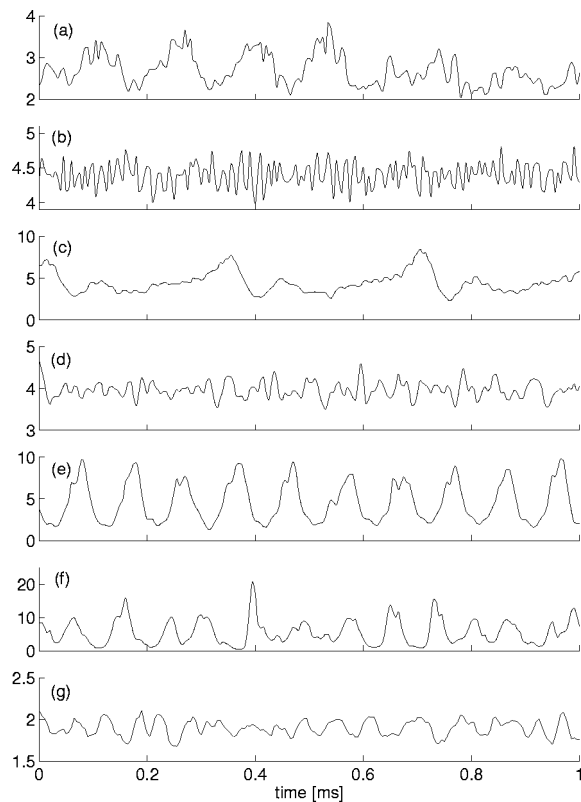


FIG. 6. Typical discharge current oscillograms of operating Regimes 1–7. The vertical axis unit is ampere (note that the vertical scales are not the same). (a)–(f) $Q_{Xe}=5$ mg/s, $I_B=4.5$ A; (g) $Q_{Xe}=2$ mg/s, $I_B=3.6$ A. (a) Regime 1. Borosil walls. $U_d=70$ V. (b) Regime 2. Alumina walls. $U_d=100$ V. (c) Regime 3. Borosil walls. $U_d=125$ V. (d) Regime 4. Borosil walls. $U_d=275$ V. (e) Regime 5. Alumina walls. $U_d=200$ V. (f) Regime 6. Silicon carbide walls. $U_d=350$ V. (g) Regime 7. Borosil walls. $U_d=600$ V.

rest of the power is mostly spread between 20–80 kHz. This frequency band corresponds to that of an ionization instability that propagates irregularly along the circumference of the channel.^{5,41} Regime 2 does not stand out in Fig. 4, but in the right columns of Fig. 2, it is clearly associated with a drop in fluctuation amplitude. See for example the cases of borosil and alumina, 100 V, or silicon carbide, 120–125 V, and the related spectra in the right panes of Fig. 3.

Regime 3: With borosil and silicon carbide walls, this regime appears in the negative resistance part of the I – V characteristics, at higher applied voltages than Regime 2. With graphite walls, this order of appearance is reversed. In Regime 3, strong and regular oscillations of the discharge current are present, with an rms amplitude that can reach about 50% of the dc current. This appears in the power spectrum as a sharp peak at low frequency (around 5 kHz) with strong harmonics up to the fourth (and possibly the fifth). These oscillations can also be observed in the discharge voltage, which leads us to relate them to the “loop”³⁷ or “contour”³⁶ oscillations described in the Russian literature. Note that the original denomination can also be translated to “circuit” oscillations,³⁸ in this context.

Regime 4: This regime appears distinctly only with borosil walls. It is located in the low-voltage part of the plateau in the I – V characteristics (see Fig. 4, in particular). The rela-

tive fluctuation amplitude is moderate (10% of the dc current). The spectrum is essentially spread over the entire range of our Fourier analysis, but a region of strong activity can be located between 10–20 kHz, its position shifting towards higher frequencies as the applied voltage is increased. Although these fluctuations are attenuated for the most part by the RLC filter of the discharge power processing unit, they somewhat follow the same frequency dependence on applied voltage as the circuit instability appearing in Regimes 3 and 5. They might then result from a weak and turbulent manifestation of the same phenomenon.

Regime 5: This regime is observed over a wide range of applied voltages in Fig. 4 (340–520 V), but only for a few operating points in Figs. 2 and 3 (e.g., borosil walls, $U_d=350$ V, alumina walls, $U_d=150$ –200 V). In all cases, this regime appears in a region of the I – V characteristic where the propellant utilization has supposedly reached a maximum. The oscillograms show strong, regular oscillations with a main frequency around 20–25 kHz, and harmonics up to the fourth can be seen in the spectra. At low applied voltages (e.g., 340 V in the configuration corresponding to Figs. 4 and 5), these oscillations are sinusoid-like. With increased applied voltage, the oscillation amplitude also increases until it almost reaches the dc value, and the oscillograms then take the shape of short current peaks alternating with periods of very low current. As in Regime 3, these oscillations are poorly filtered by the power processing unit and they can be seen in the discharge voltage, they are therefore of the “circuit” type. Their features were recovered by a hybrid transient 1D simulation of the discharge⁴² that described them as an ionization instability resulting from the “breathing” of the front of neutrals near the channel exhaust (see also Ref. 30 for a similar comparison between experiments and simulations). In another numerical study of these oscillations,⁴³ their frequency was estimated with a predator–prey model:

$$\omega \sim \frac{1}{L} (V_i V_n)^{1/2},$$

where V_i and V_n are velocities of the ions and neutrals, respectively, and L is the characteristic length of the discharge. Since V_i scales as³⁴

$$V_i \sim \left(\frac{2eU_d}{m_i} \right)^{1/2}$$

and assuming that V_n does not vary significantly with applied voltage,⁴⁰ this leads to

$$\omega \sim U_d^{1/4}.$$

This result seems to correlate the evolution of the circuit oscillation main frequency observed in Fig. 5 up to 480 V. At higher applied voltages, the decrease in frequency could be attributed to nonlinearities not taken into account in this simple model. In sum, the circuit oscillations observed in Regime 5 can be related almost unambiguously to the continuous cycle of slow injection of neutrals and fast ejection of the produced ions, now commonly called the “breathing” instability.^{38,44}

Regime 6: This high voltage regime (e.g., $U_d \geq 540$ V with borosil walls and $Q_{Xe} = 3.5$ mg/s, $U_d \geq 250$ V with alumina walls, $U_d \geq 300$ V with silicon carbide walls) is associated in the right panes of Fig. 2 and in Fig. 4 with the highest dc current values. The oscillograms are composed of periods of irregular and relatively weak fluctuations alternating with sharp peaks, and the maxima can reach over three times the corresponding dc current values. It is interesting to note that the amplitude of those peaks increases with applied voltage for all wall materials except alumina, in which case it decreases. In the power spectrum, the region of strongest activity is located around 15 kHz, moving to lower frequencies as the applied voltage is increased. These instabilities are believed to be of the “breathing” type again, but pulsed.

Regime 7: This very high voltage (higher than Regime 6) regime can be observed with the SPT100-ML only at low xenon flow rates, because of the practical limitations in discharge power. The dc current is higher than in Regime 6, the fluctuations have relatively small rms amplitudes (about 20% of the dc current) and are mostly irregular, with some features that could be related to the “breathing” instability.

Transitions from one regime to another are realized over a narrow range of applied voltages: a few volts in general. The detailed transition from weak to strong fluctuations (e.g., from Regime 4 to Regime 5) occurs as follows: first, strong current spikes appear more and more often until they merge into bursts of regular oscillations, then these bursts become longer and longer until no periods of weak fluctuations remain. In some other characterizations of the SPT100-ML, hysteresis phenomena were observed at the transitions between regimes, but they were not systematically studied.

Depending on the wall material, xenon flow rate and coil current, some of the lower voltage regimes (1–4) disappear from the I – V characteristic, or only mixed regimes (corresponding to transitions) remain.

To study the effect of the anode gas flow rate on discharge operation, several current–voltage characteristics were realized with borosil walls. As the xenon mass flow rate is decreased from 6.5 mg/s to 2.0 mg/s, the low voltage regimes (1–3) move to higher voltages, the high voltage regimes (4–7) follow the opposite direction, overall resulting in a shrinking of the operating regime spread. At the lowest flow rate studied, $Q_{Xe} = 2.0$ mg/s, the hump at low voltages and the associated regimes (2 and 3) disappear. Finally, series of measurements were made for every wall materials with fixed applied voltage and coil current ($U_d = 300$ V and $I_B = 4.5$ A), and with a mass flow rate varying between 6.5 mg/s and 2.5 mg/s. With alumina, silicon carbide and graphite, the thruster remains operating at Regime 6, the dc current and rms power both varying proportionally to the mass flow rate. With borosil, the dc current follows the same trend, but below 3.5 mg/s, the operating regime changes from 4 to 5 due to the operating envelope shrinking.

A major difference in SPT100-ML operation when the channel walls are not made of borosil is the appearance of Regime 5 at lower voltages: about 100 V with alumina and 200 V with silicon carbide and graphite instead of 350 V with borosil. In fact, borosil is the only wall material with which Regime 4 appears distinctly. With silicon carbide

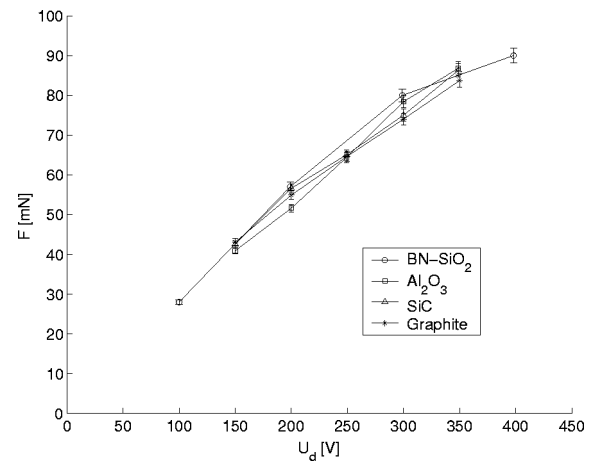


FIG. 7. Thrust of the SPT100-ML as a function of the applied voltage. Xenon flow rate: 5 mg/s. Coil current: 4.5 A.

walls, one can only note the case of $U_d = 200$ V, where a close examination of the oscillograms (not shown here) reveals that the thruster is in an intermediate regime between Regime 4 and Regime 5, with bursts of strong and regular oscillations alternating with calmer periods. Concerning alumina and graphite, if Regime 4 exists with these wall materials, it is probably out of the SPT100-ML design parameters.

To conclude this section, since all the measurement series presented in Figs. 2 and 3 include the SPT100-ML nominal operating point, we examine the similarities between our classification and Tilinin’s. Regimes 4 and IV are certainly identical, as revealed by the extended range of operation in these regimes with borosil walls ($U_d = 150$ – 325 V for Regime 4, $I_B = 3.5$ – 6.7 A for Regime IV, respectively). Regimes 6 and IIIb are probably the same (see the operation with alumina and silicon carbide walls at the nominal operating point). Common features can be found between regimes 7 and IIIa (high dc current, low level of fluctuations, presence of “breathing” instabilities), regimes 1 and II (strong “spoke” instability), regimes 2 and VI (relatively high dc current, low level of fluctuations), regimes 3 and V (strong “circuit” instabilities), respectively. As for Regime I (classical conductivity regime), in which the magnetic field is low, and consequently, the electron Larmor radius is large, it could correspond to a hypothetical Regime 8, at applied voltages higher than in Regime 7.

3. Thrust and efficiency

It is clear from Figs. 2 and 3 that the nature of the wall material has some impact on the discharge current mean value (up to 25% variation between materials) and a significant impact on the level of fluctuations (often exceeding 100% between materials). Figure 7, however, shows that the axial thrust F is less affected: a maximum relative difference of 10% is measured, whereas a discharge current difference of more than 25% can be observed at the same time. The comparison of boron nitride and a glass ceramic as channel wall materials undertaken in Ref. 19 produced similar results. As mentioned in the introduction, however, another comparison, of boron nitride and diamond,²⁰ found signifi-

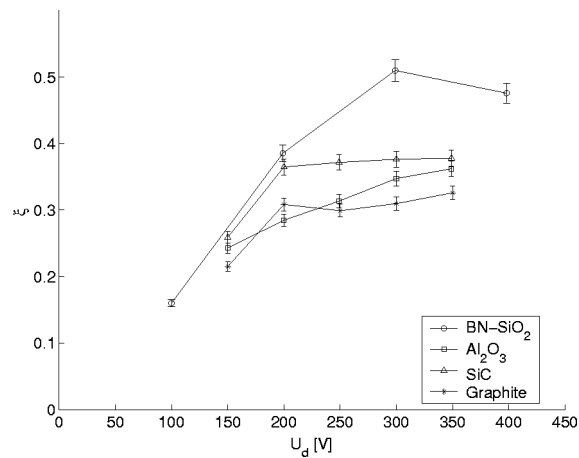


FIG. 8. Efficiency of the SPT100-ML discharge as a function of the applied voltage. Xenon flow rate: 5 mg/s. Coil current: 4.5 A.

cant differences in both the ion current (which, for a given specific impulse, is proportional to thrust, knowing that most of the ions are singly ionized in typical Hall thruster discharges^{5,45}) and the electron current, but it might also result from the unusual channel geometry (rectangular instead of annular) of the thruster used in that study. In sum, the wall material may generally have more effect on the electron dynamics than on the ionization process and the shaping of the electric field lines.

For all wall materials and various applied voltages, Fig. 8 shows the discharge efficiency, defined as

$$\xi = \frac{F^2}{2Q_{Xe}P},$$

where P is the discharge power.

It can be seen in this figure that the use of borosil clearly results in the best thrust efficiency, especially at the nominal operating point: 0.51, compared to 0.38 with silicon carbide, 0.36 with alumina and 0.31 with graphite (with $\pm 4\%$ uncertainty). On the other hand, since borosil is a mixture of boron nitride, it is not expected to have a better resistance to sputtering than the other materials.²⁰ Therefore, it can be assumed that borosil was originally chosen as channel wall material for the commercial SPT-100 mainly because of the resulting low discharge power and high thrust efficiency.

It should be cautioned again that Figs. 2–8 are only typical of the discharge behavior. However, since much efforts were taken to realize the measurements in similar test conditions, it is believed that the characterizations and the comparisons between wall materials are still relevant.

B. Wall effects on the discharge current

1. Preliminary remark on the stability of the discharge

In a Hall thruster with a classical annular channel configuration, the density of azimuthal electron current due to $\mathbf{E} \times \mathbf{B}$ drift can be expressed as

$$J_{e\theta} \approx en_e \frac{E_z}{B_r},$$

where n_e is the electron density, E_z is the axial electric field, and B_r is the radial magnetic field.

Knowing that the Hall parameter $\omega_c \tau_e \gg 1$, one can then derive the two-dimensional electron momentum equation for weakly ionized plasma to find the axial current density in the bulk,⁴⁰

$$J_{ez} \approx \frac{en_e}{\omega_c \tau_e} \frac{E_z}{B_r}.$$

For a fixed value of the magnetic field, assuming that the plasma density and the electric field do not change significantly, it can be seen that if $\omega_c \tau_e$ somehow rises above a critical value, the discharge can be sustained only if some instabilities appear in the bulk plasma and effectively reduce the Hall parameter, or if some complementary “by-pass” electron current is provided. Of course, for thrust efficiency considerations, this by-pass current should remain reasonably low.

2. Existing near-wall conductivity theories

The most elaborate theory of electron–wall interactions in Hall thruster discharges has been developed since the 1960s by Morozov, one of the major contributors to Hall thruster physics and technology. His first works on the subject¹⁷ were motivated by the need to find a supplemental mechanism to explain the higher-than-classical electron conductivity observed in Hall thruster discharges at the time,³ since Bohm diffusion⁴⁶ was not sufficient. Further developments of this near-wall conductivity theory aimed at better understanding the non-Maxwellian electron energy distribution observed in the discharge⁴⁷ and the structure and stability of the Debye sheath. It was also suggested that the main source of wall scattering could be related to surface inhomogeneities, provided that their characteristic size was at least comparable to the Debye length. Indeed, as mentioned in the Introduction, experiments showed that increasing the wall surface roughness resulted in a significant augmentation of discharge current values over the whole current–voltage characteristic of the stationary plasma thruster.¹⁶

In our experiments, the tolerance requirements on the sets of channel walls included a surface roughness under 2 μm , which is two orders of magnitude smaller than the Debye length. Moreover, it was verified after the end of the tests that the erosion due to ion bombardment did not significantly increase the surface roughness of the channel walls. Therefore, the near-wall conductivity induced by surface inhomogeneities can be neglected.

Other theories developed in the former Soviet Union³³ emphasized the role of secondary electron emission (SEE) by the channel walls due to electron bombardment. This secondary electron process can be involved in the Hall thruster discharge through two effects:

- (1) Channel walls with high SEE yields σ give rise to high cross-field electron conductivity, since a large fraction of the incident electrons are returned to the plasma with a new guiding drift along the direction of the electric field.⁴³
- (2) The secondary electrons have energies that are, on average, lower than the primaries, resulting in a cooling of the discharge,²³ a lower ion production rate and therefore, a lower ion current.

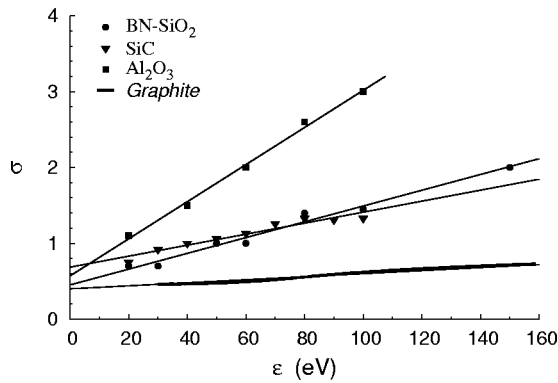


FIG. 9. Experimental total secondary emission yield as a function of the primary electron energy. For insulating ceramics, the yields were measured on samples of the tested channel wall materials (Ref. 52). The data for graphite are taken from Pedgley and McCracken (Ref. 53). Dashed lines give linear approximations of those yields.

This second effect is expected to be quenched for energies of the primaries high enough to result in a space-charge saturation (SCS) of the sheath. The SCS phenomenon was first suggested in the case of stationary plasma thrusters by Baitin *et al.*,⁴⁸ and later analyzed in details by Jolivet and Roussel.⁴⁹

It is noteworthy that the SEE mechanisms were not given much attention in Morozov's works, although they were not excluded from the general formulation of his near-wall conductivity theory.³⁶ One can only mention that in Ref. 50, a condition is given for having an "efficient" (i.e., providing a sufficient by-pass current, as explained in Sec. III B 1) near-wall conductivity: that the SEE yield, $\sigma \geq 1$. Following the same argument, it was suggested in Ref. 18 that a quartz or steel coating on the channel walls of an "efficient" stationary plasma thruster can reduce σ below unity, causing the onset of bulk plasma fluctuations.

In the next section, we will estimate the impact of SEE on the SPT100-ML discharge current dc value. Note that electron emission induced by ion bombardment is not believed to play a significant role, since it is in general negligible for energies below 1 keV. For example, the yield of MgO (a good emitter used in plasma display panels) under Xe^+ impact with energies up to 300 eV is of the order of 0.01.⁵¹

Finally, in the case of conducting walls, the SEE effects are expected to be weaker than for dielectrics due to the usually lower values of σ . It has been shown,³³ however, that conducting floating walls act in general as a negatively biased electrode for most of the channel length, except in the exit plane where a large electron current is drained.

3. Dielectric materials

The effective secondary electron emission yields of the three nonconducting materials that we tested were measured⁵² using similar experimental conditions and apparatus, for incident electron energies ranging from 20 to 100 eV. The data for all three materials are shown in Fig. 9.

The cross-field electron current due to electron-wall collisions can be estimated using the near-wall conductivity law,¹⁷ which also constitutes an approximation of Ohm's law in a strong magnetic field:

$$I_w = \frac{\sigma \Gamma_{ew}}{\omega_c^2} \frac{e^2}{m_e} E_z,$$

where Γ_{ew} is the flux density of electrons towards the walls per unit of axial length, ω_c is the electron cyclotron frequency.

When the yield σ is below the critical value⁴⁹ $\sigma_{SCS} \approx 0.98$, the flux density Γ_{ew} can be determined by considering the balance between the ion current density Γ_{iw} towards the walls and the electron currents collected and emitted by the walls:

$$\Gamma_{iw} = \Gamma_{ew} - \sigma \Gamma_{ew}.$$

Assuming that the ions enter the sheath with Bohm velocity⁵⁴ $V_B \approx \sqrt{kT_e/m_i}$, the following relationship can be derived:

$$\Gamma_{ew} = \Gamma_{iw} \frac{1}{1 - \sigma} \approx 2\pi(R_1 + R_2)n_e \sqrt{\frac{kT_e}{m_i}} \frac{1}{1 - \sigma},$$

where R_1 and R_2 are the radii of the innermost and outermost walls, respectively, and n_e is defined at the sheath edge.

As the applied voltage is increased or the magnetic field decreased, the mean electron energy eventually reaches the threshold for which $\sigma = \sigma_{SCS}$. For $\sigma > \sigma_{SCS}$, space charge effects result in a partial trapping of secondary electrons in the vicinity of the walls and in a limitation of the electron current flowing through the sheath.⁵⁵ In a modern stationary plasma thruster configuration, this space charge saturation is expected to occur first locally, close to the exit plane (where the electron temperature is highest), and rapidly spread over the whole acceleration region of the channel as the bulk electron energy increases. The flux density Γ_{ew} in the SCS regime is given by⁵⁵

$$\Gamma_{ew} \approx 2\pi(R_1 + R_2)n_e \sqrt{\frac{kT_e}{2\pi m_e}} \exp(-1.02).$$

Under such an assumption, and using the following typical plasma parameters in the high B -field region:^{5,32,36,40} $n_e = 1.5 \cdot 10^{17} \text{ m}^{-3}$; $E_z = 3 \cdot 10^4 \text{ V} \cdot \text{m}^{-1}$; $T_e = 20 \text{ eV}$; $B = 15 \text{ mT}$. The axial electron current for $U_d = 300 \text{ V}$ can be estimated as follows: alumina and silicon carbide channels, assuming $\sigma > 0.98$ in the high B -field region:

$$I_w \approx 2.6 \text{ A};$$

borosil channel, assuming $\sigma = 0.8$ in the high B -field region:

$$I_w \approx 0.18 \text{ A}.$$

The value of σ in the second case is deliberately overestimated to emphasize the effect of space charge saturation: although it is a continuous function of σ , the electron current becomes significant only when σ closely approaches or exceeds σ_{SCS} . These estimates are of course approximate, but they do match the orders of magnitudes observed in experiments, provided that the ion current amounts to about 3.5 A.

The effect of dielectric walls on the mean discharge current can therefore be described as *potentially* large at high discharge voltage (depending on the material) even though the wall conductivity can be very modest for low SEE materials.

At low discharge voltages, the near-wall conductivity due to SEE must be negligible or moderate even with materials like alumina because of the low electron temperature and therefore, the low value of σ . Moreover, a close examination of Fig. 2 reveals that for $U_d \leq 100$ V, the dc current is actually lower with alumina walls than with borosil walls (by about 10%). This corroborates a recent experimental study of a stationary thruster with boron nitride and alumina walls⁵⁶ and could be explained by the cooling effect becoming dominant over the near-wall conductivity effect in the ionization branch of the I - V characteristic.

4. Graphite

The SEE yield of graphite was found in the literature⁵³ and is shown in Fig. 9. For this material, despite variations from one author to another, most published experimental data consistently report a low σ . Consequently, the SEE induced near-wall current must be even lower than with borosil. On the other hand, the electrical conductivity of graphite strongly modifies the picture given in the case of dielectric walls. The short-circuit current through the walls³³ is neutralized by the ion current collected all over the surface of the channel exposed to the plasma. Assuming that the ions enter the sheath with Bohm velocity, the short-circuit current can therefore be approximated by

$$I_{sc} \approx e \int_S n_e \sqrt{\frac{kT_e}{m_i}} dS,$$

where $S = 2\pi(R_1 + R_2)L$ is the area of the plasma-facing surfaces inside the channel.

This relationship emphasizes the fact that the short-circuit current is determined by the plasma parameters inside the whole channel, in contrast with the case of dielectric walls where the wall-induced current is almost exclusively determined by the plasma parameters inside the high magnetic field region. In estimating the short-circuit current we shall thus use values of plasma density and electron temperature averaged over the whole plasma-facing surfaces. Assuming for instance, $\langle n_e \rangle = 4 \cdot 10^{17} \text{ m}^{-3}$; $\langle T_e \rangle = 10$ eV, the short-circuit current can be estimated as $I_{sc} = 2.3$ A.

It seems thus likely that the large currents obtained with graphite arise from the electrical conductivity of this material and are not related to the near-wall conductivity due to SEE, which is indeed expected to be negligible in regard to the shielding effect of negatively biased walls.

5. Photoelectricity

There is also a possibility that the walls play a role in enhancing electron conductivity through photoelectron emission. Xenon discharges are indeed known as strong ultraviolet (UV) radiation sources, in a wavelength band that often corresponds to a high photoemission yield. An interesting related effect in drift tube discharges was analyzed by Specht *et al.*⁵⁷ when they investigated the discrepancies between, on the one hand, measured ionization and excitation coefficients for noble gases at low electric fields, and on the other hand calculations based on the transport equations. Their analysis revealed that near the excitation or ionization thresholds, the

secondary electrons emitted by the wall due to metastable radiations could not be neglected against the bulk plasma electrons. It is also relevant to our study that silicon carbide and alumina are sometimes used in high efficiency photoelectrodes for UV detectors.

In the case of SPTs running with xenon, let us consider for example the Xe I emission around $\lambda \approx 100$ – 150 nm, where several strong lines are present⁵⁸ as a result of de-excitation of excited atoms (energy $E_\lambda \approx 8.5$ – 11.5 eV) towards the fundamental energy level. These excited levels can be populated directly by electron collisions, by deexcitation of neutrals from higher levels, or by ion–electron recombination. Let us consider the pessimistic case, where the UV radiation energy in the bulk plasma is imprisoned and lost to other processes. Then, only the photons emitted within a distance approximately equal to the optical depth d of the plasma can reach the wall and contribute to photoelectricity.

Assuming Doppler broadening, the optical depth d inside the discharge is given by⁵⁹

$$\frac{1}{d} = 5.4 \times 10^{-9} \lambda \sqrt{\frac{\mu}{T_n}} n_n,$$

where μ is the atomic mass and T_n is the temperature of the emitters. Taking $\mu = 131$ (xenon), $\lambda \approx 120$ nm, and typical values inside the channel, near the exit, $T_n \approx 0.06$ eV, $n_n \approx 10^{12} \text{ cm}^{-3}$, we obtain $d \approx 3$ mm.

Farther than a distance d from the wall, the photons are quickly reabsorbed. Moreover, going axially towards the anode, more than halfway from the channel exit plane the temperature of the electrons is too low for them to create enough photon emitters. We will then consider only the UV photons that are emitted within a volume V delimited by those boundaries:

$$V = 0.5L \pi (R_2^2 - (R_2 - d)^2 + (R_1 + d)^2 - R_1^2),$$

where L is the channel length. Assuming that the number of emitters is given by the Boltzmann fraction, the photoelectron current can be estimated:

$$I_{pe} = \kappa e A_{nm} n_n V \exp\left(-\frac{E_\lambda}{T_e}\right) \gamma,$$

where κ is a view factor conservatively estimated to 0.2, A_{nm} is the Einstein coefficient of the emission, whose average value in this case is⁵⁸

$$A_{nm} \approx 4 \cdot 10^8 \text{ s}^{-1},$$

and γ is the photoelectron quantum yield of the walls (i.e., the number of electrons emitted per incident photon), which can vary within several orders of magnitude depending on the type of material and the incident radiation wavelength. Absolute measurements of γ for the materials that we tested are difficult to find in the literature. In the case of alumina, we can refer to a standard windowless photodiode⁶⁰ for finding at this wavelength $\gamma \approx 2\%$, and finally the total photoelectron current,

$$I_{pe} \approx 1.6 \text{ A}.$$

It should be noted that this current is spread over the channel surface and cannot be simply added as a direct contribution to the discharge current. However, with so many approximations, it is also possible that we actually underestimated I_{pe} . In any case, the near-wall current due photoelectron emission could be not negligible, although it has apparently never been considered in the Hall thruster literature.

6. Concluding remarks on discharge operation

In light of the preceding discussion, it is now possible to return to the SPT100-ML operating regimes illustrated in Figs. 2–6 and make some additional comments, starting with dielectric walls.

In the ionization branch of the I – V characteristic (Regimes 1–3), the discharge operation features observed with borosil, silicon carbide and alumina walls result probably from the complex interactions between the ionization-related plasma instabilities (e.g., “spoke”), the cooling effect and possibly some near-wall conductivity due to SEE (especially for high-yield materials like alumina), which all influence, or are influenced by, the electron energy transport and balance.

At higher applied voltages, it is tempting to attribute the extended range of efficient operation observed only with borosil, i.e., the low level of dc current and fluctuations (Regime 4), to the low SEE yield of this material. This is consistent with the dc current jumps observed in Fig. 4 between $U_d=520$ – 540 V and in Fig. 2, top left, between $I_B=3.5$ – 3.7 A, and also the higher dc current with silicon carbide and alumina walls at the nominal operating point, which could all be caused by the space charge saturation of the channel wall sheath that occurs as σ approaches unity. Note also that in the cases of Regime 4 presented here, a rapid estimate shows that the level of anomalous conductivity due to plasma instabilities is low. Furthermore, under those assumptions, the processes involved in Regime 6 would be as follows. Due to the SCS of the wall sheath, the electron temperature is no longer moderated by the SEE-induced cooling effect. Due to the high electron temperature, the flow of neutrals is rapidly transformed into an ion current, which results in a strong “breathing” instability and high discharge current peaks. Between those peaks, the neutral density and consequently the classical electron conductivity is low, and the discharge is sustained with near-wall conductivity and/or anomalous conductivity.

It remains unclear what influence, if any, the walls have on the transitions between Regimes 4 and 5, and between Regimes 6 and 7, which are mainly characterized by the progressive apparition or disparition of the “breathing” instability. Since this instability is also related to the ionization process, we suspect, however, that the SEE from the walls does play a role.

The case of graphite walls is more complex, as witnessed for example by the order of appearance of Regimes 2 and 3 being reversed. Moreover, at the nominal operating point, one cannot simply invoke the low SEE, as in Ref. 18, to explain the high level of instabilities in the discharge, since the short-circuit created by the conducting walls is ex-

pected to provide more than a minimum by-pass current (as described in Sec. III B 1). Rather, it is probable that the situation is similar to that of alumina and silicon carbide walls, i.e., most of the electrons do not reach the walls and their energy is not moderated. This would be due, however, not from the SCS of the wall sheath but more simply, by the wall potential remaining uniform over the whole length of the channel (since graphite is an electric conductor) and at a low value, close to the cathode potential.

Finally, one can wonder what would happen if the channel wall material was dielectric but the SEE yield was even lower than that of borosil. This could be the case of diamond, whose SEE yield increases when it is doped with boron.⁶¹ As mentioned before, experiments with such channel walls showed that the discharge current and ion current are both lower than with boron nitride walls.²⁰ More recent studies of the same thruster⁶² also revealed an unusual operating mode with diamond walls and nominal discharge parameters (Regime 4 with boron nitride walls), where strong discharge current pulses are present, as in Regime 6, but the dc current is very low: 0.1 A, compared to 1 A with boron nitride walls. Questions remain, however, about the role played by the channel geometry of this particular thruster—linear instead of annular—in discharge operation.

IV. SUMMARY

We have presented an extensive characterization of a stationary plasma thruster that was operated with four different wall materials: three dielectric ceramics and graphite. The data revealed that wall material can be added to the list, given in Ref. 38, of parameters that can strongly influence Hall thruster discharge operation. On the other hand, thrust is only moderately affected.

We gave an overview of the wall effects that are potentially at play in Hall thruster operation: near-wall conductivity due to surface inhomogeneities (believed to be negligible in our experiments), near-wall conductivity due to secondary electron emission (SEE) under electron bombardment, cooling of the discharge due to SEE, space charge saturation of the wall sheath at high SEE yields, current conduction inside the graphite walls, near-wall conductivity due to photoelectron emission.

Borosil (a boron nitride–silica mixture) is the only material of the four tested that allows running the thruster in a low current fluctuation, high thrust efficiency regime. This is apparently the main motivation behind the use of this wall material, and more generally, of boron nitride based ceramics, on stationary plasma thruster flight models. We suggest that these good performance are due to the low SEE yield of borosil and the fact that it is electrically insulating.

ACKNOWLEDGMENTS

The authors are most grateful to Pascal Lasgorceix, Stephane Béchu, and Alain Hauser for their technical assistance on the PIVOINE facility, and to Virginie Viel-Inguibert for providing the results of experimental measurements of secondary electron emission yields. N.G. and S.B. also wish to thank Professor M. A. Cappelli from Stan-

ford University for many stimulating discussions, and in particular for suggesting the importance of the photoelectric effect.

This work was done within the frame of the French Research Group "Plasma Propulsion for Space Systems (GDR No 2232 CNRS/CNES/SNECMA/ONERA)." N.G. is supported by a fellowship from the European Space Agency. S.B. also wishes to acknowledge the support given by the Polish Committee for Scientific Research (KBN) in the frame of Projects Nos. 8-T07A-028-21 and 8-T12D-015-21.

- ¹A. I. Morozov, *23rd International Electric Propulsion Conference* (The Electric Rocket Propulsion Society, Worthington, OH, 1993), IEPC-93-101.
- ²H. R. Kaufman, *AIAA J.* **21**, 78 (1985).
- ³G. S. Janes and R. S. Lowder, *Phys. Fluids* **9**, 1115 (1966).
- ⁴C. Brown and E. A. Pinsky, *AIAA J.* **3**, 853 (1965).
- ⁵V. V. Zhurin, H. R. Kaufman, and R. S. Robinson, *Plasma Sources Sci. Technol.* **8**, R1 (1999).
- ⁶A. I. Morozov, Yu. V. Esipchuk, A. M. Kapulkin, V. A. Nevrovskii, and V. A. Smirnov, *Sov. Phys. Tech. Phys.* **17**, 482 (1972).
- ⁷R. X. Meyer, *AIAA J.* **5**, 2057 (1967).
- ⁸L. A. Artsimovich, I. P. Andronov, Yu. V. Esipchuk *et al.*, *Kosm. Issled.* **12**, 451 (1974) (in Russian).
- ⁹M. Martinez-Sanchez and J. Pollard, *J. Propul. Power* **14**, 688 (1998).
- ¹⁰V. Kim, G. Popov, B. Arkhipov *et al.*, *27th International Electric Propulsion Conference* (The Electric Rocket Propulsion Society, Worthington, OH, 2001), IEPC-01-005.
- ¹¹H. R. Kaufman, *AIAA/JSASS/DGLR 16th International Electric Propulsion Conference* (American Institute of Aeronautics and Astronautics, Washington, D.C., 1982), AIAA-82-1919.
- ¹²G. M. Plank, H. R. Kaufman, and R. S. Robinson, *AIAA/JSASS/DGLR 16th International Electric Propulsion Conference* (American Institute of Aeronautics and Astronautics, Washington, D.C., 1982), AIAA-82-1920.
- ¹³C. E. Garner, J. E. Polk, L. C. Pless, K. D. Goodfellow, and J. R. Brophy, *23rd International Electric Propulsion Conference* (The Electric Rocket Propulsion Society, Worthington, OH, 1993), IEPC-93-91.
- ¹⁴T. Randolph, V. Kim, H. Kaufman, K. Kozubsky, V. Zhurin, and M. Day, *23rd International Electric Propulsion Conference* (The Electric Rocket Propulsion Society, Worthington, OH, 1993), IEPC-93-93.
- ¹⁵J. M. Sankovic, J. A. Hamley, and T. W. Haag, *23rd International Electric Propulsion Conference* (The Electric Rocket Propulsion Society, Worthington, OH, 1993), IEPC-93-94.
- ¹⁶A. I. Bugrova, A. I. Morozov, and V. K. Kharchevnikov, *Sov. J. Plasma Phys.* **16**, 849 (1990).
- ¹⁷A. I. Morozov, *Zh. Prikl. Mekh. Tekh. Fiz.* (in Russian) **3**, 19 (1968).
- ¹⁸A. I. Bugrova, A. V. Desyatkov, A. I. Morozov, and V. K. Kharchevnikov, *Plasma Phys. Rep.* **4**, 302 (1996).
- ¹⁹J. Ashkenazy, Y. Raitses, and G. Appelbaum, *Phys. Plasmas* **5**, 2055 (1998).
- ²⁰N. B. Meezan, N. Gascon, and M. A. Cappelli, *27th International Electric Propulsion Conference* (The Electric Rocket Propulsion Society, Worthington, OH, 2001), IEPC-01-039.
- ²¹V. Egorov, V. Kim, V. Kozlov *et al.*, *24th International Electric Propulsion Conference* (The Electric Rocket Propulsion Society, Worthington, OH, 1995), IEPC-95-45.
- ²²A. Zhakupov, S. Khartov, L. Latyshev, *3rd International Conference on Spacecraft Propulsion* (ESA Publication Division, Noordwijk, Netherlands, 2000), p. 827.
- ²³Y. Raitses, L. A. Dorf, A. A. Litvak, and N. J. Fisch, *J. Appl. Phys.* **88**, 1263 (2000).
- ²⁴A. Cadiou, C. Gelas, F. Darnon, L. Jolivet, and N. Pillet, *27th International Electric Propulsion Conference* (The Electric Rocket Propulsion Society, Worthington, OH, 2001), IEPC-01-008.
- ²⁵C. Pérot, N. Gascon, A. Hauser, S. Béchu, P. Lasgorceix, and M. Dudeck, *21st Symposium on Rarefied Gas Dynamics* (Cepadues, Toulouse, 1998), p. 633.
- ²⁶A. Bouchoule, C. Philippe-Kadlec, M. Prioul *et al.*, *Plasma Sources Sci. Technol.* **10**, 364 (2001).
- ²⁷D. Valentian and N. Maslennikov, *25th International Electric Propulsion Conference* (The Electric Rocket Propulsion Society, Worthington, OH, 1997), IEPC-97-134.
- ²⁸S. Béchu, C. Pérot, N. Gascon, P. Lasgorceix, A. Hauser, and M. Dudeck, *35th AIAA/ASME/ASEE Joint Propulsion Conference* (American Institute of Aeronautics and Astronautics, Washington, D.C., 1999), AIAA-99-2567.
- ²⁹M. Touzeau, M. Prioul, S. Roche *et al.*, *Plasma Phys. Controlled Fusion* **42**, B323 (2000).
- ³⁰N. Gascon, C. Pérot, G. Bonhomme *et al.*, *35rd AIAA/ASME/ASEE Joint Propulsion Conference* (AIAA, Washington, D.C., 1999), AIAA-99-2427.
- ³¹S. Barral, N. Gascon, K. Makowski, Z. Peradzyński, and M. Dudeck, *Phys. Plasmas* **10**, 4137 (2003).
- ³²A. Bishaev, V. Gavryushin, V. Kim *et al.*, *4th All-Union Conference on Plasma Accelerators and Ion Injectors* (Energoatomizdat, Moscow, 1978), p. 57 (in Russian).
- ³³V. Egorov, V. Kim, A. Semenov, and I. Shkarban, *Ionnyye Inzhektory i Plasmennyye Uskoriteli* (Energoatomizdat, Moscow, 1990), p. 56 (in Russian).
- ³⁴V. Kim, *J. Propul. Power* **14**, 736 (1998).
- ³⁵P. D. Welch, *IEEE Trans. Audio Electroacoust.* **AU-15**, 70 (1967).
- ³⁶A. I. Morozov and V. V. Savelyev, *Rev. Plasma Phys.* **21**, 203 (2000).
- ³⁷G. N. Tilinin, *Sov. Phys. Tech. Phys.* **22**, 974 (1977).
- ³⁸E. Y. Choueiri, *Phys. Plasmas* **8**, 1411 (2001).
- ³⁹A. M. Bishaev and V. Kim, *Sov. Phys. Tech. Phys.* **23**, 1055 (1978).
- ⁴⁰N. B. Meezan, W. A. Hargus, Jr., and M. A. Cappelli, *Phys. Rev. E* **63**, 026410 (2001).
- ⁴¹Yu. V. Esipchuk, A. I. Morozov, G. N. Tilinin, and A. V. Trofimov, *Sov. Phys. Tech. Phys.* **18**, 928 (1974).
- ⁴²J.-P. Boeuf and L. Garrigues, *J. Appl. Phys.* **84**, 3541 (1998).
- ⁴³J. M. Fife, M. Martinez-Sanchez, and J. Szabo, *33rd AIAA/ASME/ASEE Joint Propulsion Conference* (American Institute of Aeronautics and Astronautics, Washington, D.C., 1997), AIAA-97-3051.
- ⁴⁴E. Chesta, C. M. Lam, N. B. Meezan, D. P. Schmidt, and M. A. Cappelli, *IEEE Trans. Plasma Sci.* **29**, 582 (2001).
- ⁴⁵L. B. King and A. D. Gallimore, *J. Propul. Power* **16**, 1086 (2000).
- ⁴⁶D. Bohm, E. H. S. Burhop, and H. S. W. Massey, *The Characteristics of Electrical Discharges in Magnetic Fields* (McGraw-Hill, New York, 1949), p. 13.
- ⁴⁷A. I. Bugrova, A. V. Desyatkov, and A. I. Morozov, *Sov. J. Plasma Phys.* **18**, 501 (1992).
- ⁴⁸A. V. Baitin, L. I. Elizarov, A. A. Ivanov, and M. Bacal, in *Proceedings of the 27th International Electric Propulsion Conference* (The Electric Rocket Propulsion Society, Worthington, OH, 1995), IEPC-95.
- ⁴⁹L. Jolivet and J.-F. Roussel, *3rd International Conference on Spacecraft Propulsion* (ESA Publication Division, Noordwijk, Netherlands, 2000), p. 367.
- ⁵⁰A. I. Morozov, *Sov. Phys. Tech. Phys.* **32**, 901 (1987).
- ⁵¹K. S. Moon, J. Lee, and K. Whang, *J. Appl. Phys.* **86**, 4049 (1999).
- ⁵²V. Viel-Inguibert, *28th International Electric Propulsion Conference* (The Electric Rocket Propulsion Society, Worthington, OH, 2003), IEPC-03-258.
- ⁵³J. M. Pedgley and G. M. McCracken, *Plasma Phys. Controlled Fusion* **35**, 397 (1993).
- ⁵⁴D. Bohm, *The Characteristics of Electrical Discharges in Magnetic Fields* (McGraw-Hill, New York, 1949), p. 77.
- ⁵⁵G. D. Hobbs and J. A. Wesson, *Plasma Phys.* **9**, 85 (1967).
- ⁵⁶N. Gascon and M. A. Cappelli, *28th International Electric Propulsion Conference* (The Electric Rocket Propulsion Society, Worthington, OH, 2003), IEPC-03-028.
- ⁵⁷L. T. Specht, S. A. Lawton, and T. A. DeTemple, *J. Appl. Phys.* **51**, 166 (1980).
- ⁵⁸J. Reader and C. H. Corliss, *CRC Handbook of Chemistry and Physics*, 79th ed. (CRC Press, Boca Raton, 1998).
- ⁵⁹H. R. Griem, *Plasma Spectroscopy* (Academic, New York, 1966).
- ⁶⁰L. R. Canfield and N. Swanson, *Far Ultraviolet Detector Standards*, Natl. Bur. Stand. Spec. Publ. 250-2 (U.S. GPO, Washington, D.C., 1987), p. 12.
- ⁶¹J. B. Miller and G. R. Brandes, *J. Appl. Phys.* **82**, 4538 (1997).
- ⁶²N. Gascon, C. Thomas, W. Hermann, and M. A. Cappelli, *28th International Electric Propulsion Conference* (The Electric Rocket Propulsion Society, Worthington, OH, 2003), IEPC-03-027.